

Vibrational Analyses of Di-μ-oxo-Bridged Manganese Dimers Based on Density Functional Theory Calculations. Theoretical Evaluation of Mn–O Vibrations of the Mn-Cluster Core for Photosynthetic Oxygen-Evolving Complex

Koji Hasegawa*,† **and Taka-aki Ono***,††

Laboratory for Photo-Biology (I), RIKEN Photodynamics Research Center, 519-1399 Aoba, Aramaki, Aoba-ku, Sendai 980-0845

Received September 13, 2005; E-mail: kojihase@riken.jp

Normal coordinate analyses of di-μ-oxo-bridged $[Mn_2^{III,III}(\mu\text{-}O)_2(ND_3)_8]^{2+}$, $[Mn_2^{III,IV}(\mu\text{-}O)_2(ND_3)_8]^{3+}$, and $[Mn_2^{IV,IV}(\mu\text{-}O)_2(ND_3)_8]^{4+}$ dimers were carried out systematically based on force-constants obtained by B3PW91 hybrid density functional theory (DFT) calculations on a broken-symmetry electronic state. Calculation results indicated that all Mn–O–Mn/Mn–O stretch vibrations are found at 697–387 cm^{-1} with the strongest infrared (IR) intensities occurring at 620, 697, and 615 cm^{-1} for $Mn_2^{III,III}$, $Mn_2^{III,IV}$, and $Mn_2^{IV,IV}$ dimers, respectively, which are compatible with experimental data. These strong IR bands were assigned to the Mn–O–Mn asymmetric stretch 1 (B_{3u} vibration) for the equivalent $Mn_2^{III,III}$ and $Mn_2^{IV,IV}$ dimers with D_{2h} symmetry, and the Mn^{IV}–O symmetric stretch (A_1 vibration) for the mixed-valence $Mn_2^{III,IV}$ dimer with C_{2v} symmetry. Based on the results of calculations, the reported ^{18}O-sensitive IR bands in the low-frequency S_2/S_1 spectrum in a photosynthetic oxygen-evolving complex (OEC) were assigned to the Mn^{IV}–O asymmetric stretch (B_2 vibration) in the di-μ-oxo-bridged $Mn_2^{III,IV}$ dimer moiety for the S_1-state Mn-cluster core and the Mn–O–Mn asymmetric stretch 1 (B_{3u} vibration) in the di-μ-oxo-bridged $Mn_2^{IV,IV}$ dimer moiety in the S_2-state Mn-cluster core.

The photosynthetic oxidation of water to molecular oxygen occurs through five intermediate states denoted S_n ($n = 0$–4), by which a molecular oxygen is released during the S_3–(S_4)–S_0 transition. This reaction is catalyzed by an oxygen-evolving complex (OEC) composed of a tetranuclear Mn-cluster plus one Ca^{2+} ion located on the lumenal side of the D1 protein of photosystem II (PSII).[1–4] Although recent X-ray crystallographic studies at 3.2- to 3.5-Å resolution identified electron densities corresponding to Mn and/or Ca ions in the OEC,[5,6] individual metal ions could not be resolved; therefore, the structure of the Mn-cluster in the OEC has not been determined. Various spectroscopic techniques, including electron paramagnetic resonance (EPR), X-ray absorption structure (XAS), and Fourier-transform infrared (FTIR), have been applied to OEC for characterizing the structural and functional properties of OEC, and the changes that occur in these properties during S-state cycling. Especially, the S_1-to-S_2 transition process has been extensively investigated because the S_2 state can be generated from the dark-stable S_1 state by continuous illumination of PSII samples at low temperature or in the presence of PSII inhibitors.

EPR and X-ray absorption near edge structure (XANES) studies have suggested that the oxidation states of the Mn-cluster in the S_1 and S_2 states are $Mn_4^{III,III,IV,IV}$ or $Mn_4^{III,III,III,III}$, and $Mn_4^{III,IV,IV,IV}$ or $Mn_4^{III,III,III,IV}$, respectively.[1,6–9] The S_2-state Mn-cluster gives rise to a multiline EPR signal at $g = 2$ arising from a total spin $S_T = 1/2$ ground state of the Mn-cluster core with at least one strong-antiferromagnetically coupled $Mn_2^{III,IV}$ dimer moiety, which is mainly responsible for the 18–20 lines hyperfine structure.[1–4,10,11] Extended X-ray absorption fine structure (EXAFS) studies have indicated the presence of two or three ≈2.7-Å Mn–Mn distances and one ≈3.3-Å Mn–Mn and Mn–Ca distance in the S_1-state Mn-cluster; these distances change little in the S_2 state.[9,12,13] These studies suggest that the S_1- and S_2-state Mn-clusters consist of two or three di-μ-oxo-bridged Mn dimer moieties and one mono-μ-oxo-bridged Mn dimer and Mn–Ca moieties.

Vibrational modes for the Mn–oxo and Mn–ligand interactions should appear in a low-frequency region (800–100 cm^{-1}) in the Mn-cluster, based on reported vibrational assignments for various metal complexes.[14] Low-frequency (650–350 cm^{-1}) FTIR spectra for the S_2/S_1 difference have been obtained for PSII samples from spinach,[15–18] *Synechocystis* PCC6803,[19–22] and *Thermosynechoccous elongatus*.[23] The spectra exhibited relatively strong difference bands at 650–550 cm^{-1} and weak bands at 550–350 cm^{-1}. Deuterium-insensitive and ^{18}O-sensitive bands have been observed at 638, 617, 606, and 594 cm^{-1}, which were assigned to Mn–O–Mn vibrations of the Mn-cluster in *T. elongatus*.[23] Corresponding ^{18}O-sensitive bands have been observed in the spinach spectra at 625, 609, and 596 cm^{-1}, and the 625 and 606 cm^{-1} bands tentatively ascribed to Mn–O–Mn vibrations in the S_1 and S_2

† Present Address: Molecular Membrane Biology Laboratory, RIKEN, 2-1 Hirosawa, Wako 351-0198

†† Present Address: Department of Biomolecular Functional Engineering, Faculty of Engineering, Ibaraki University, 4-12-1 Nakanarusawa-cho, Hitachi 316-8511

Published on the web July 4, 2006; doi:10.1246/bcsj.79.1025

states, respectively, by assuming a 10–12 cm^{-1} downshift of the bands caused by the ^{18}O isotope.[16] Strong infrared (IR) bands of di-μ-oxo-bridged $Mn_2^{III,IV}$ and $Mn_2^{IV,IV}$ dimer complexes have been observed at 694–604 cm^{-1},[18,24–29] despite there being no data for the $Mn_2^{III,III}$ dimer. Therefore, these bands may originate from vibrational changes of the di-μ-oxo-bridged Mn dimer moiety due to Mn oxidation upon the S_1-to-S_2 transition. However, detailed vibrational assignments for the bands in terms of Mn oxidation are difficult because of the lack of information on the IR and Raman properties of di-μ-oxo-bridged Mn dimer complexes, which are structurally identical but differ in the oxidation state of the Mn ions with the exception of only one resonance Raman study for a di-μ-oxo-bridged Mn dimer.[30]

Structure, electronic/chemical properties, vibrational frequencies, and IR intensities of a molecule can be obtained quantitatively by density functional theory (DFT) calculations. Although vibrational frequencies were evaluated based on DFT calculations in some multinuclear Mn complexes[31,32] or based on empirical force-constants in Mn dimer complexes,[33] no ab initio vibrational calculations were performed for di-μ-oxo-bridged Mn dimers. DFT calculation using a broken-symmetry approach can be applicable to describe an electronic state for antiferromagnetically coupled transition-metal dimer complexes whose electronic configurations have α and β spin orbitals opposite to each other.[34–44] Therefore, this approach has been used to elucidate the structure, electronic properties, antiferromagnetism, and EPR parameters of various antiferromagnetically coupled Mn dimers, including the di-μ-oxo-bridged dimer,[34–44] and to evaluate potential water oxidation chemistry in OEC based on the dimer models.[37,41,43–47]

In the present study, we performed B3PW91 hybrid DFT calculations to obtain force-constants and IR intensities for di-μ-oxo-bridged $Mn_2^{III,III}$, $Mn_2^{III,IV}$, and $Mn_2^{IV,IV}$ dimers using the broken-symmetry approach. Based on the calculation results, the effects of oxidation state on Mn–O stretch vibrations in the di-μ-oxo-bridged Mn dimers were evaluated systematically by normal coordinate analyses, and possible vibrational assignments for the observed S_2/S_1 low-frequency FTIR bands in OEC are discussed.

Computational Methods

All calculations were performed using Gaussian03[48] and Jaguar 5.5[49] program packages. Geometry optimizations, spin population analyses, and Cartesian force-constant and IR intensity calculations for di-μ-oxo-bridged Mn dimers were carried out without symmetry restriction using the open-shell hybrid DFT method along with Becke's three-exchange hybrid functional[50] combined with Perdew–Wang 1991 local and GGA-II non-local functionals[51,52] (B3PW91). The standard 6-31+G(d) basis set for H, N, and O atoms and a double-ζ type effective core potential[53] (LANL2DZ) for the Mn ion were used. For the calculations, a di-μ-oxo-bridged octahedral Mn dimer with ammonia ligands $[Mn_2(\mu\text{-}O)_2(NH_3)_8]^{n+}$ (n = 2–4) (see Fig. 1) with a $Mn_2^{III,III}$, $Mn_2^{III,IV}$, or $Mn_2^{IV,IV}$ dimer oxidation state was chosen as the simplest model, because it is well characterized theoretically[34,38] and reduces CPU resources to a minimum. Total charges for the $Mn_2^{III,III}$, $Mn_2^{III,IV}$, and $Mn_2^{IV,IV}$ dimers were +2, +3, and +4, respectively. For

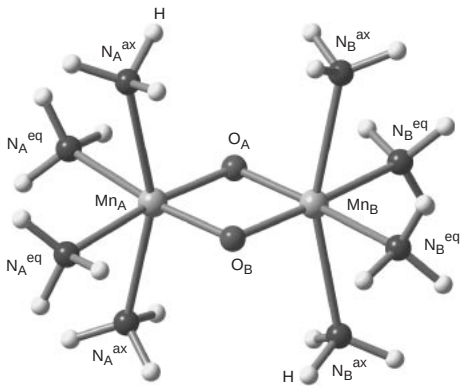

Fig. 1. A model of the di-μ-oxo-bridged Mn dimer used for the calculations.

Table 1. Internal and Normal Coordinates for Mn_2O_2 Core Vibrations

Mn_2O_2 core vibrations	
Internal coordinates	Definition[a)]
R1	$\Delta r(Mn_A–O_A)$
R2	$\Delta r(Mn_B–O_A)$
R3	$\Delta r(Mn_A–O_B)$
R4	$\Delta r(Mn_B–O_B)$
R5	$\Delta\delta(O_A–Mn_A–O_B)$
R6	$\Delta\delta(Mn_A–O_B–Mn_B)$
R7	$\Delta\delta(O_B–Mn_B–O_A)$
R8	$\Delta\delta(Mn_B–O_A–Mn_A)$
R9	$\Delta\tau(O_B–Mn_A–O_A–Mn_B)$
R10	$\Delta\tau(O_A–Mn_B–O_A–Mn_A)$
R11	$\Delta\tau(O_A–Mn_A–O_B–Mn_B)$
R12	$\Delta\tau(O_A–Mn_B–O_B–Mn_A)$
Normal coordinates	
Q1 (Mn–O–Mn s st 1)	$(R1+R2+R3+R4)/2$
Q2 (Mn–O–Mn as st 1)	$(R1-R2+R3-R4)/2$
Q3 (Mn–O–Mn s st 2)	$(R1-R2-R3+R4)/2$
Q4 (Mn–O–Mn as st 2)	$(R1+R2-R3-R4)/2$
Q1′ (Mn_A–O s st)	$(R1+R3)/\sqrt{2}$
Q2′ (Mn_A–O as st)	$(R1-R3)/\sqrt{2}$
Q3′ (Mn_B–O s st)	$(R2+R4)/\sqrt{2}$
Q4′ (Mn_B–O as st)	$(R2-R4)/\sqrt{2}$
Q5 (Mn–O–Mn def)	$(R5-R6+R7-R8)/2$
Q6 (Mn–O–Mn tor)	$(R9-R10+R11-R12)/2$

a) r, δ, and τ refer to distance, angle, and dihedral angle, respectively. Abbreviations for vibrations: as, asymmetric; s, symmetric; st, stretching; def, deformation; tws, twisting.

normal coordinate analysis, 12 internal and 6 normal coordinates for Mn–O–Mn vibrations were defined as shown in Table 1, in which Q1–Q6 were used for an equivalent dimer with D_{2h} symmetry and Q1′–Q4′, Q5 and Q6 represented a mixed-valence dimer with C_{2v} symmetry. The eigenvectors of the normal coordinates for Mn–O–Mn/Mn–O stretches are illustrated in Fig. 2. The normal coordinates for 8 Mn–NH_3 stretches, 16 Mn–NH_3 bendings, 16 asymmetric and 8 symmetric NH_3 stretches, 16 asymmetric and 8 symmetric NH_3 deformations, 16 NH_3 rockings, and 8 NH_3 twistings are defined in the Supporting Information. The calculated Cartesian

force-constant matrix was transformed to that for the molecular symmetry coordinate. Vibrational frequencies and potential energy distributions (PED) were calculated using a modified NCTB program.[54,55] The calculated vibrational frequencies were uniformly scaled by a factor of 0.89. No imaginary frequency was found for the $Mn_2^{III,III}$, $Mn_2^{III,IV}$, and $Mn_2^{IV,IV}$ dimers, confirming the stability of the optimized geometries (Tables S1–S6).

Results

Optimized Geometries and Spin Populations for Di-μ-oxo-Bridged Mn Dimers. Table 2 lists the optimized geometry parameters for the di-μ-oxo-bridged $Mn_2^{III,III}$, $Mn_2^{III,IV}$, and $Mn_2^{IV,IV}$ dimers on broken-symmetry states and experimental data for di-μ-oxo-bridged Mn dimer complexes, which contain only nitrogen atoms as ligands (with the exception of an oxygen atom in a di-μ-oxo-bridge). The calculated Mn–Mn and Mn–O distances were similar to those obtained experimentally. Calculated Mn–Mn distances were 2.712, 2.742, and 2.781 Å for the $Mn_2^{III,III}$, $Mn_2^{III,IV}$, and $Mn_2^{IV,IV}$ dimers, respectively, indicating that the oxidation of Mn^{III} to Mn^{IV} lengthens the Mn–Mn distance by 0.030–0.039 Å. In contrast, the Mn–O distance for the $Mn_2^{III,III}$ dimer (1.815 Å) was longer than that for the $Mn_2^{IV,IV}$ dimer (1.795 Å). The Mn^{III}–O distance of the $Mn_2^{III,IV}$ dimer (1.862 Å) was longer than that of the $Mn_2^{III,III}$ dimer (1.815 Å), while the Mn^{IV}–O distance was shorter in the $Mn_2^{III,IV}$ dimer (1.746 Å) than in the $Mn_2^{IV,IV}$ dimer (1.795 Å). The Mn^{III}–N^{ax} distances were much longer than their Mn–N^{eq} distances, due to the Jahn–Teller effect in the $3d^4$ orbital configuration for Mn^{III}, indicating that the Jahn–Teller axes of the Mn^{III} ions were perpendicular to the Mn_2O_2 plane. The Mn–N^{eq} distance in the $Mn_2^{IV,IV}$ dimer was longer than those in the $Mn_2^{III,III}$ and $Mn_2^{III,IV}$ dimers.

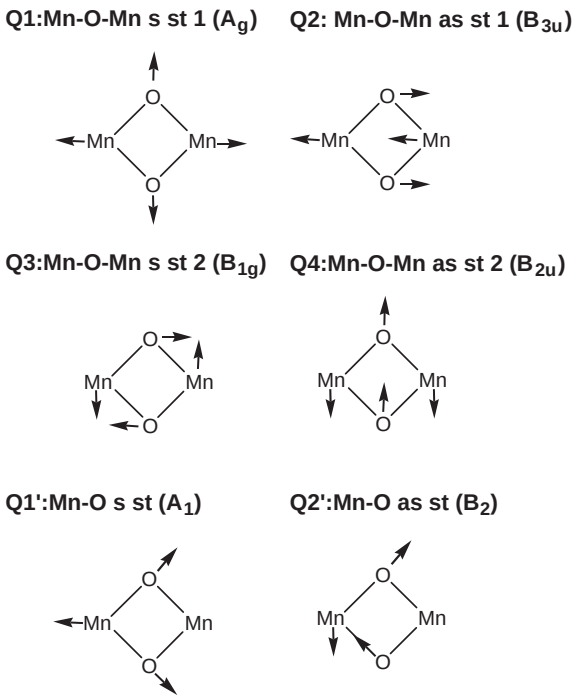

Fig. 2. Four eigenvectors for normal modes of Mn–O–Mn stretch vibrations for the equivalent Mn dimer and two eigenvectors of four Mn–O stretch vibrations for the mixed-valence Mn dimer.

Table 3 lists Mulliken spin populations for the optimized Mn dimers. Spin populations ($|\rho|$) of the Mn^{III} ions were 4.167 and 4.211 for the $Mn_2^{III,III}$ and $Mn_2^{III,IV}$ dimers, respectively, and those for the Mn^{IV} ions were 2.935 and 3.202 in the $Mn_2^{III,IV}$ and $Mn_2^{IV,IV}$ dimers, respectively, which are greater than $|\rho|$ (<0.128) on hydrogen, oxygen, or nitrogen atoms. Total spin populations for the $Mn_2^{III,III}$, $Mn_2^{III,IV}$, and $Mn_2^{IV,IV}$ dimers was calculated as 0.000, 1.000, and 0.000, respectively, in consistent with the total spin values S_T, 0, 1/2 and 0 for the pure spin state of a di-μ-oxo-bridged Mn dimer whose Mn ions are strong-antiferromagnetically coupled each other. The expected value $\langle S_T^2 \rangle$ was found to be 4.056, 3.785, and 3.044 for $Mn_2^{III,III}$, $Mn_2^{III,IV}$, and $Mn_2^{IV,IV}$ dimers, respectively. These values were not equal to those for the pure spin state, but were close to the sum of the formal spin for Mn^{III} ($S = 2$) and Mn^{IV} ($S = 3/2$), indicating that the electronic states of these dimers are weakly overlapped magnetic couplings.[35] Optimized geometries and spin populations of the $Mn_2^{III,III}$, $Mn_2^{III,IV}$, and $Mn_2^{IV,IV}$ dimers were similar to those obtained from other DFT methods.[34,38]

Table 2. Optimized Geometry Parameters for $[Mn_2(\mu\text{-}O)_2(NH_3)_8]^{n+}$ ($n = 2$–4)

	Bond lengths/Å					
	Mn_A^{III}–Mn_B^{III}		Mn_A^{III}–Mn_B^{IV}		Mn_A^{IV}–Mn_B^{IV}	
	calc	exp[a)]	calc	exp[b)]	calc	exp[c)]
Mn_A–Mn_B	2.712	2.674–2.707	2.742(+0.030)[d)]	2.643–2.741	2.781(+0.039)[e)]	2.671–2.746
Mn_A–O	1.815	1.815–1.863	1.862(+0.048)	1.835–1.890	1.795(−0.067)	1.746–1.822
Mn_A–N_A^{ax}	2.461	2.312–2.469	2.446(−0.015)	2.207–2.362	2.067(−0.379)	1.987–2.018
Mn_A–N_A^{eq}	2.176	2.159–2.108	2.156(−0.020)	2.044–2.151	2.150(−0.006)	2.001–2.090
Mn_B–O	1.815	1.815–1.863	1.746(−0.068)	1.771–1.870	1.795(+0.049)	1.746–1.822
Mn_B–N_B^{ax}	2.461	2.312–2.469	2.056(−0.405)	2.004–2.093	2.067(+0.011)	1.987–2.018
Mn_B–N_B^{eq}	2.176	2.159–2.108	2.167(−0.009)	2.027–2.163	2.150(−0.017)	2.001–2.090

a) Experimental range for $Mn_2^{III,III}$ dimer complexes (HEWJIC, KAWLID, VEZHIR, VEZHOX, RUXZAL, and RUXZEP) obtained from the Cambridge Structural Database. b) Experimental range for $Mn_2^{III,IV}$ dimer complexes (FOGHAKG, GAMFEK, GEPSUP, GIXKON, HEWJEY, HEWJOI, SEJXUA, YEMCIC, ZAXNER, and ZUKHES) obtained from the Cambridge Structural Database. c) Experimental range for $Mn_2^{IV,IV}$ dimer complexes (FEBKOM, KEGNUF, SICBAH, and SOZVEI) obtained from the Cambridge Structural Database. d) Shift from the $Mn_2^{III,III}$ dimer value. e) Shift from the $Mn_2^{III,IV}$ dimer value.

Table 3. Mulliken Spin Populations for $[Mn_2(\mu\text{-}O)_2(NH_3)_8]^{n+}$ ($n = 2$–4)

	Oxidation states		
	Mn_A^{III}–Mn_B^{III}	Mn_A^{III}–Mn_B^{IV}	Mn_A^{IV}–Mn_B^{IV}
	Mulliken spin populations		
Mn_A	4.167[a)]	4.211	3.202
Mn_B	−4.167	−2.935	−3.202
O	0.000	−0.193	0.000
N_A^{ax}	−0.014	0.010	−0.081
N_A^{eq}	−0.099	−0.103	−0.128
N_B^{ax}	0.014	0.062	0.081
N_B^{eq}	0.099	0.095	0.128
H[b)]	0.000	0.018	0.000
Total[c)]	0.000	1.000	0.000
	Total spin values S_T		
S_T^{calc} d)	0.000	0.500	0.000
S_T^{pure} e)	0	1/2	0
	Expected values of S_T^2 operator		
$\langle S_T^2\rangle^{calc}$ f)	4.056	3.785	3.044
$\langle S_T^2\rangle^{pure}$ g)	0	3/4	0
Spin contamination[h)]	4.056	3.035	3.044

a) Positive and negative signs indicate populations of alpha and beta spins, respectively. b) Sum of spin populations for all hydrogen atoms. c) Sum of spin populations for all atoms. d) Evaluated total spin value for the calculated spin state. e) Total spin value for the pure spin state. f) Expected value of S_T^2 operator for the calculated spin state. g) Expected value of S_T^2 operator for the pure spin state, $S_T^{pure}(S_T^{pure}+1)$. h) $\langle S_T^2\rangle^{calc} - \langle S_T^2\rangle^{pure}$.

Vibrational Assignments for Di-μ-oxo-Bridged Mn Dimers. Mn–O vibrational frequencies for hydrated and deuterated $Mn_2^{III,III}$, $Mn_2^{III,IV}$, and $Mn_2^{IV,IV}$ dimers were obtained successfully using the B3PW91 method (Tables 4 and S1–S6). The frequencies obtained for the Mn–O stretch and NH_3 rocking vibrations overlapped and were strongly coupled at 750–550 cm^{-1} in the hydrated dimers $[Mn_2(\mu\text{-}O)_2(NH_3)_8]^{n+}$ ($n =$ 2–4) (Tables S4–S6). For the deuterated dimers, the effects of the Mn valence changes on Mn–O vibrational frequency can be evaluated easily because the ND_3 modes were decoupled from the Mn–O vibrations. In Table 4, vibrations assigned primarily to Mn–O stretch vibrations with >10% potential energy distribution (PED) are listed, together with data reported for several model complexes, and the IR intensities were classified as strong, weak, and very weak or inactive. DFT calculations indicated dominant Mn–O stretch vibrations were in the region of 697–387 cm^{-1}. Vibrations for Mn–O–Mn deformation and torsion were found at 380–70 cm^{-1} and were sensitive to the oxidation state of the Mn ions (Tables S1–S6), although these vibrations were essentially IR inactive.

In the $Mn_2^{III,III}$ dimer, the Mn–O–Mn asymmetric stretch 1 and 2 (B_{3u} and B_{2u} vibrations) occurred at 620 and 575 cm^{-1} with strong and weak IR intensities, respectively, and IR-inactive Mn–O–Mn symmetric stretch vibrations (A_g and B_{1g} vibrations) occurred at 592 and 436 cm^{-1}. These Mn–O–Mn stretches were downshifted by 21–31 cm^{-1} in Mn–^{18}O–Mn to 600–400 cm^{-1}, although no IR or Raman data for a di-μ-oxo-bridged $Mn_2^{III,III}$ dimer complex has been reported. In the $Mn^{III,IV}$ dimer, Mn–O stretch vibrations occurred at 697, 629, 542, 443, and 387 cm^{-1}. The strongest 697 cm^{-1} vibration was assigned predominantly to the Mn^{IV}–O symmetric stretch (A_1 vibration), which was downshifted by 32 cm^{-1} by ^{18}O substitution. Notably, the IR spectra reported for di-μ-oxo-bridged $Mn_2^{III,IV}$ dimer complexes contained a strong IR band at 694–679 cm^{-1}, depending on the ligand.[25–27] Furthermore, spectra of the complexes in 53 or 51% enriched $H_2{}^{18}O$ showed an additional band at frequencies lower by 12 or 9 cm^{-1},[25,27] coinciding with the 15-cm^{-1} downshift predicted by the calculation for ($Mn_2{}^{16}O{}^{18}O$) in the $Mn_2^{III,IV}$ dimer. Therefore, the IR band reported in the di-μ-oxo-bridged $Mn_2^{III,IV}$ dimer complexes may be assigned to the Mn^{IV}–O symmetric stretch. Calculations indicated other weak-intensity IR active vibrations that were assigned to Mn^{IV}–O asymmetric and Mn^{III}–O symmetric stretches (B_2 and A_1 vibrations) at 629 and 542 cm^{-1}, respectively, in the $Mn_2^{III,IV}$ dimer. However, spectra reported for the complexes contain no prominent IR band, except for vibrations at 694–679 cm^{-1}. These bands may show very weak IR intensities depending on Mn_2O_2 geometry and ligands. IR-inactive Mn^{III}–O asymmetric stretch vibrations (B_2 vibrations) occurred at 443 and 387 cm^{-1}, which were downshifted by 9 cm^{-1} upon ^{18}O substitution. The overall features of Mn–O–Mn stretch vibrations for the $Mn_2^{IV,IV}$ dimer were similar to those for the $Mn_2^{III,III}$ dimer, as expected from their structural symmetry, although their individual IR positions and activities were somewhat different. A strong IR band was observed at 692–604 cm^{-1} in the di-μ-oxo-bridged $Mn_2^{IV,IV}$ dimer complexes.[24,25,28,30] Table 4 shows that Mn–O–Mn asymmetric stretch 1 (B_{3u} vibration, 615 cm^{-1}) was the major IR-active vibration, while Mn–O–Mn asymmetric stretch 2 (B_{2u} vibration) with contribution from ND_3 rocking vibrations was found at 580 cm^{-1}, but with much weaker intensity for the $Mn_2^{IV,IV}$ dimer. The predominant vibrations for Mn–O–Mn symmetric stretch 1 and 2 (A_g and B_{1g} vibrations) were found at 629 and 478 cm^{-1}, but these were IR inactive. Therefore, the reported band is likely to be due to the Mn–O–Mn asymmetric stretch 1 (B_{3u} vibration).

Discussion

In this study, vibrational analyses of di-μ-oxo-bridged Mn dimers with three oxidation states were carried out systematically by B3PW91 hybrid DFT calculations to investigate the effect of Mn oxidation on the Mn–O–Mn/Mn–O stretch IR bands of the Mn dimer. The calculation results indicated that the strongest IR absorptions were assigned to the Mn–O–Mn asymmetric stretch 1 (B_{3u} vibration) at 620 cm^{-1} for the $Mn_2^{III,III}$ dimer and at 615 cm^{-1} for the $Mn_2^{IV,IV}$ dimer, and the Mn^{IV}–O symmetric stretch (A_1 vibration) at 697 cm^{-1} for the $Mn_2^{III,IV}$ dimer. The strongest band appears at a much higher frequency in the $Mn_2^{III,IV}$ dimer than in the $Mn_2^{III,III}$ and $Mn_2^{IV,IV}$ dimers. The frequencies and extent of the ^{18}O-isotope downshifts of theses bands produced by the calculations are generally compatible with those of the observed IR bands in the di-μ-oxo-bridged $Mn_2^{III,IV}$ dimer[25–27] and $Mn_2^{IV,IV}$ dimer[24,25,29] complexes, although no data was availa-

Table 4. Vibrational Frequencies, Isotope Shifts, and Assignments of Mn–O Stretch Vibrations of $[Mn_2(\mu\text{-}O)_2(ND_3)_8]^{n+}$ ($n = 2$–4)

ν	Frequencies/cm^{-1} calc[b]	exp[c]	Assignments (PED, %)[a]
	$Mn_2^{III,III}$		
$\nu1$	620(306s)[d]{−15}[e][−31][f]		Mn–O–Mn as st 1 (98)
$\nu2$	592(0i){−15}[−31]		Mn–O–Mn s st 1 (81), Mn–O–Mn def (15)
$\nu3$	575(147w){−10}[−21]		Mn–O–Mn as st 2 (79)
$\nu4$	436(19i){−10}[−25]		Mn–O–Mn s st 2 (80)
	$Mn_2^{III,IV}$		
$\nu1$	697(214s){−15}[−32]	679(−9),[g] 686,[h] 688(−12),[i] 694[j]	Mn^{IV}–O s st (90)
$\nu2$	629(109w){−15}[−22]		Mn^{IV}–O as st (75)
$\nu3$	542(157w){−15}[−27]		Mn^{III}–O s st (77), Mn–O–Mn def (15)
$\nu4$	443(5i){−4}[−9]		Mn^{III}–O as st (34), as $N_B{}^{eq}D_3$ rock (16), Mn^{IV}–O as st (15)
$\nu5$	387(2i){−4}[−9]		Mn^{III}–O as st (41), as $N_A{}^{eq}D_3$ rock (28), as $N_B{}^{eq}D_3$ rock (16)
	$Mn_2^{IV,IV}$		
$\nu1$	629(0i){−12}[−26]		Mn–O–Mn s st 1 (71), Mn–O–Mn def (14)
$\nu2$	615(503s){−10}[−23]	604,[k] 609,[l] 619,[m] 642,[n] 692[o]	Mn–O–Mn as st 1 (86)
$\nu3$	580(74w){−6}[−11]		Mn–O–Mn as st 2 (51), s $N_A{}^{ax}D_3$ rock (13), as $N_B{}^{ax}D_3$ rock (13)
$\nu4$	478(0i){−9}[−17]		Mn–O–Mn s st 2 (65), as $N_A{}^{eq}D_3$ rock (14), as $N_B{}^{eq}D_3$ rock (14)
		625(−12)[p]	Mn^{IV}–O as st of S_1 state $Mn_2^{III,IV}$ moiety in OEC
		606(−10)[p]	Mn–O–Mn as st 1 of S_2 state $Mn_2^{IV,IV}$ moiety in OEC

a) Potential energy distributions (%) are given in parenthesis. b) Calculated frequencies were uniformly scaled by a factor of 0.89. c) Observed strong IR band and ^{18}O shift in parenthesis of di-μ-oxo-bridged Mn dimer complexes. d) IR intensity in parenthesis calculated in km mol^{-1}; s, w, and i represent expected strong, weak, and inactive or very weak IR intensities, respectively. e) Shift of Mn–$^{16}O^{18}O$–Mn from vibrations in Mn–$^{16}O_2$–Mn dimer given in brackets. f) Shift of Mn–$^{18}O_2$–Mn from vibrations in Mn–$^{16}O_2$–Mn dimer given in square brackets. g) $[Mn_2^{III,IV}(\mu\text{-}O)_2(14\text{-}aneN_4)_2]^{3+}$.[27] h) $[Mn_2^{III,IV}(\mu\text{-}O)_2(phen)_4]^{3+}$.[26] i) $[Mn_2^{III,IV}(\mu\text{-}O)_2(bipy)_4]^{3+}$.[25] j) $[Mn_2^{III,IV}(\mu\text{-}O)_2(tren)_2]^{3+}$.[26] k) $[Mn_2^{IV,IV}(\mu\text{-}O)_2(salen)_2]^{4+}$.[29] l) $[Mn_2^{IV,IV}(\mu\text{-}O)_2(salipn)_2]^{4+}$.[29] m) $[Mn_2^{IV,IV}(\mu\text{-}O)_2(salbn)_2]^{4+}$.[29] n) $[Mn_2^{IV,IV}(\mu\text{-}O)_2(busaltm)_2]^{4+}$.[24] o) $[Mn_2^{IV,IV}(\mu\text{-}O)_2(phen)_4]^{4+}$.[25] p) Observed Mn–O–Mn vibrational band and ^{18}O shift in parentheses in the low-frequency S_2/S_1 spectrum of spinach PSII.[16] Abbreviations for vibrations: as, asymmetric; s, symmetric; st, stretching; def, deformation; rock, rocking; bend, bending.

ble for the di-μ-oxo-bridged $Mn_2^{III,III}$ dimer complex. Experimental data for di-μ-oxo-bridged Mn dimer complexes with identical ligands but different oxidation states are required for a detailed evaluation of the present DFT calculations.

The calculations indicated that the appearance of Mn–O–Mn asymmetric stretch 2 bands for the $Mn_2^{III,III}$ and $Mn_2^{III,IV}$ dimers and Mn^{III}–O symmetric and Mn^{IV}–O asymmetric stretch bands for the $Mn_2^{III,IV}$ dimer were of weak IR intensity. Some Mn–O IR bands observed at 510–425 cm^{-1} in adamantan-like Mn_4O_6 complexes[56] may be related to the weak bands produced by the calculations. Resonance Raman spectra of di-μ-oxo-bridged dimer complexes with the 2-(2′-pyridyl)benzimidazole ligand contained one strong resonance band at 695–694 cm^{-1}, both in $Mn_2^{III,IV}$ and $Mn_2^{IV,IV}$ oxidation states, which was downshifted by 29 cm^{-1} due to ^{18}O substitution.[30] As shown in Table 4, the observed downshift was close to that calculated for Mn–O stretches from the $Mn_2^{III,IV}$ dimer and Mn–O–Mn stretches for the $Mn_2^{IV,IV}$ dimer, which include no ligand vibrational modes. Considering the inverse relation between IR and Raman activity, the Mn^{IV}–O asymmetric stretch (B_2 vibration) at 629 cm^{-1} in the $Mn_2^{III,IV}$ dimer and Mn–O–Mn symmetric stretch (A_g vibration) at 629 cm^{-1} in the $Mn_2^{IV,IV}$ dimer could be possible candidates for the resonance Raman band observed. Some differences between the calculated (629 cm^{-1}) and observed (695–694 cm^{-1}) frequency may be due to a difference in ligands.

Low-frequency S_2/S_1 light-induced FTIR difference spectra of OEC have been reported at 650–350 cm^{-1}, where relatively strong difference bands were observed at 650–550 cm^{-1} with weak difference bands at 550–350 cm^{-1}.[16–23] The low-frequency S_2/S_1 difference spectrum was due mainly to changes in the Mn-cluster cores involving bridging oxygen atoms upon Mn oxidation, despite contributions from changing interactions between the Mn-cluster and its ligands, including substrate water, amino acid side groups, and peptide backbones. It was proposed that ^{18}O-sensitive 625 and 606 cm^{-1} bands with weak and strong IR intensities are attributable to S_1 and S_2 state Mn–O–Mn vibrations, respectively.[16] The S_1 and S_2 state Mn-cluster cores are thought to consist of two or three di-μ-oxo-bridged Mn dimer moieties and a mono-μ-oxo-bridged Mn dimer.[9,12,13] The oxidation states of the S_1 and S_2 state Mn-cluster cores are $Mn_4^{III,III,IV,IV}$ or $Mn_4^{III,III,III,III}$ and $Mn_4^{III,IV,IV,IV}$ or $Mn_4^{III,III,III,IV}$ respectively,[1,6–9] but the Mn–Mn and Mn–O/N distances in the Mn-cluster core change little during the S_1-

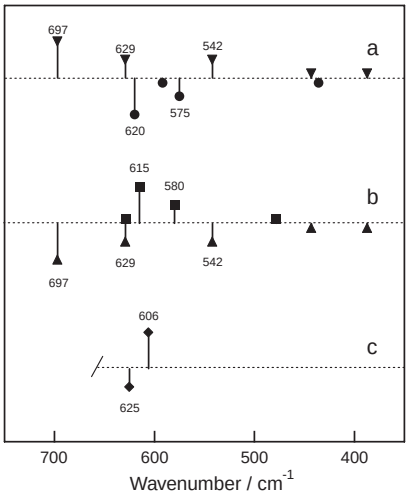

Fig. 3. IR band changes of Mn–O–Mn and Mn–O stretch vibrations of the di-μ-oxo-bridged Mn dimer upon Mn oxidation from Mn^{III} to Mn^{IV} based on calculation results: (a) oxidation from $Mn_2^{III,III}$ (negative bands) to $Mn_2^{III,IV}$ (positive bands); (b) oxidation from $Mn_2^{III,IV}$ (negative bands) to $Mn_2^{IV,IV}$ (positive bands); (c) S_2/S_1 FTIR difference bands for Mn–O–Mn vibrations in OEC;[16] the S_1 and S_2 bands correspond to negative and positive bands, respectively. See Table 4 for calculation results.

to-S_2 transition,[9,12,13] indicating that skeletal and coordination structures of the Mn-cluster core are well preserved in spite of an oxidation of the Mn ion during the transition.

According to the group frequency concept in vibrational spectroscopy, it is not an extravagant idea that the spectrum for the di-μ-oxo-bridged dimer moiety appears in that of the Mn-cluster in OEC. Therefore, the observed Mn–O–Mn vibrational bands in the light-induced S_2/S_1 FTIR difference spectrum may be interpreted by the spectral changes induced by the valence changes from $Mn_2^{III,III}$ to $Mn_2^{III,IV}$ or from $Mn_2^{III,IV}$ to $Mn_2^{IV,IV}$ in the di-μ-oxo-bridged dimer moiety. Then, we tried to assign the reported low-frequency S_1 and S_2 bands to the modes of the di-μ-oxo-bridged Mn dimers obtained by the present DFT calculations.

Figure 3 shows the calculated IR difference spectra upon oxidation of $Mn_2^{III,III}$ to $Mn_2^{III,IV}$ (a) and $Mn_2^{III,IV}$ to $Mn_2^{IV,IV}$ (b) for the Mn–O–Mn/Mn–O stretch vibrations in the di-μ-oxo-bridged Mn dimers. The IR intensities are represented by bars of varying lengths as classified in Table 4. The positive and negative bands correspond to $Mn_2^{III,IV}$ and $Mn_2^{III,III}$ dimers in spectrum (a), while the positive and negative bands in spectrum (b) correspond to $Mn_2^{IV,IV}$ and $Mn_2^{III,IV}$ dimers. Spectrum (c) shows Mn–O–Mn vibrations for the S_1 and S_2 state Mn-cluster at 625(−) and 606(+) cm^{-1} proposed from the S_2/S_1 FTIR difference spectrum of OEC.[16] The S_2 band was downshifted by 19 cm^{-1} compared to the S_1 band. This change can be reproduced by combining the negative 629 cm^{-1} and positive 615 cm^{-1} bands for the $Mn_2^{IV,IV}/Mn_2^{III,IV}$ difference, as shown in spectrum (b); other combinations of bands could not easily reproduce the S_1 and S_2 bands. Therefore, the S_1 band at 625 cm^{-1} and S_2 band at 606 cm^{-1} are assigned to the Mn^{IV}–O asymmetric stretch in the di-μ-oxo-bridged $Mn_2^{III,IV}$ dimer moiety and the Mn–O–Mn asymmetric stretch 1 in the di-μ-oxo-bridged $Mn_2^{IV,IV}$ dimer moiety in the Mn-cluster core, respectively.

The $Mn_2^{IV,IV}/Mn_2^{III,IV}$ difference spectrum shows weak IR intensity bands at 580(+) and 542(−) cm^{-1}. The reported S_2/S_1 FTIR difference spectrum showed several ^{18}O-sensitive bands in this frequency region that were difficult to assign to the S_1 or S_2 state due to other overlapping bands. The 625 and 606 cm^{-1} bands were downshifted by 10–12 cm^{-1} upon ^{18}O substitution.[16] This shift is consistent with the theoretical values obtained upon replacement of one of the bridging oxygen atoms by ^{18}O. The 10–12 cm^{-1} downshift is understandable even when both of the bridging oxygen atoms are replaced with ^{18}O, as long as the contribution of the Mn–O stretch to the bands (PED) is <50%. However, this is an unlikely scenario because the S_2/S_1 difference spectra at 630–600 cm^{-1} are minimally affected by ^{15}N labeling of PSII and only slightly affected by ^{13}C labeling,[20] indicating that the 630–600 cm^{-1} bands are due mainly to Mn–O vibrations. It is worthwhile to note in this context that the Mn–O stretch vibrations for mono-μ-oxo-bridged Mn dimer complexes appear at 712–717 and 559–566 cm^{-1}.[47,57] As no prominent bands existed for the S_2/S_1 difference in the OEC spectra in the 712–717 cm^{-1} region,[19] the contribution of vibrations from mono-μ-oxo-bridged Mn moiety to the S_2/S_1 difference spectrum in the region of 700–570 cm^{-1} can be excluded.

In conclusion, the present DFT calculations identified several Mn–O–Mn/Mn–O stretch vibrations at 697–387 cm^{-1} with strong, weak, and very weak/inactive IR intensities for the di-μ-oxo-bridged $Mn_2^{III,III}$, $Mn_2^{III,IV}$, and $Mn_2^{IV,IV}$ dimers and their positions were dependent on the oxidation state of the Mn ions in a manner compatible with the reported IR bands in some Mn complexes. We conclude that the ^{18}O-sensitive S_1 band at 625 cm^{-1} and S_2 band at 606 cm^{-1} deduced from the low-frequency S_2/S_1 FTIR difference spectrum of OEC[16] are assignable to the Mn^{IV}–O asymmetric stretch (B_2 vibration) in the di-μ-oxo-bridged $Mn_2^{III,IV}$ dimer moiety in the S_1 state Mn-cluster core and the Mn–O–Mn asymmetric stretch 1 (B_{3u} vibration) in the di-μ-oxo-bridged $Mn_2^{IV,IV}$ dimer moiety in the S_2 state Mn-cluster core, respectively.

This work was supported by grants for the Frontier Research System and Special Postdoctoral Researchers Programs (to KH) at RIKEN, and a Grand-in-Aid for Young Scientists (B) (No. 17770102) (to KH) from MEXT of Japan.

Supporting Information

The Supporting Information contains full vibrational assignments for di-μ-oxo-bridged Mn dimers, $[Mn_2(\mu\text{-}O)_2(ND_3)_8]^{n+}$ and $[Mn_2(\mu\text{-}O)_2(NH_3)_8]^{n+}$ ($n = 2$–4), based on B3PW91 hybrid DFT calculations, and the definitions of normal coordinates for NH_3 vibrations. This material is available free of charge on the web at http://www.csj.jp/journals/bcsj/.

References

1 R. J. Debus, *Biochim. Biophys. Acta* **1992**, *1102*, 269.
2 G. Renger, *Biochim. Biophys. Acta* **2001**, *1503*, 210.
3 C. Goussias, A. Boussac, A. Rutherford, *Philos. Trans. R. Soc. London, Ser. B* **2002**, *357*, 1369.
4 J. P. McEvoy, G. W. Brudvig, *Phys. Chem. Chem. Phys.*

2004, *6*, 4754.
5 K. N. Ferreira, T. M. Iverson, K. Maghlaoui, J. Barber, S. Iwata, *Science* **2004**, *303*, 1831.
6 B. Loll, J. Kern, W. Saenger, A. Zouni, J. Biesiadka, *Nature* **2005**, *438*, 1040.
7 W. Ruttinger, G. C. Dismukes, *Chem. Rev.* **1997**, *97*, 1.
8 V. K. Yachandra, *Philos. Trans. R. Soc. London* **2002**, *357*, 1347.
9 J. Messinger, *Phys. Chem. Chem. Phys.* **2004**, *6*, 4764.
10 G. C. Dismukes, Y. Siderer, *Proc. Natl. Acad. Sci. U.S.A.* **1981**, *78*, 274.
11 S. Mukhopadhyay, S. K. Mandal, S. Bhaduri, W. H. Armstrong, *Chem. Rev.* **2004**, *104*, 3981.
12 J. H. Robblee, R. M. Cinco, V. K. Yachandra, *Biochim. Biophys. Acta* **2001**, *1503*, 7.
13 H. Haumann, C. Müller, P. Liebisch, L. Iuzzolino, J. Dittmer, M. Grabolle, T. Neisius, W. Meyer-Klaucke, H. Dau, *Biochemistry* **2005**, *44*, 1894.
14 G. Socrates, *Infrared and Raman Characteristic Group Frequencies*, John Wiley & Sons Ltd., Chichester, **2001**, pp. 323–327.
15 H.-A. Chu, M. T. Gardner, J. P. O'Brien, G. T. Babcock, *Biochemistry* **1999**, *38*, 4533.
16 H.-A. Chu, H. Sackett, G. T. Babcock, *Biochemistry* **2000**, *39*, 14371.
17 H.-A. Chu, M. T. Gardner, W. Hillier, G. T. Babcock, *Photosynth. Res.* **2000**, *66*, 57.
18 H.-A. Chu, W. Hillier, N. A. Law, G. T. Babcock, *Biochim. Biophys. Acta* **2001**, *1503*, 69.
19 H.-A. Chu, R. J. Debus, G. T. Babcock, *Biochemistry* **2001**, *40*, 2312.
20 Y. Kimura, N. Mizusawa, A. Ishii, T. Yamanari, T.-a. Ono, *Biochemistry* **2003**, *42*, 13170.
21 N. Mizusawa, Y. Kimura, A. Ishii, T. Yamanari, S. Nakazawa, H. Teramoto, T.-a. Ono, *J. Biol. Chem.* **2004**, *279*, 29622.
22 Y. Kimura, N. Mizusawa, T. Yamanari, A. Ishii, T.-a. Ono, *J. Biol. Chem.* **2005**, *280*, 2078.
23 Y. Kimura, A. Ishii, T. Yamanari, T.-a. Ono, *Biochemistry* **2005**, *44*, 7613.
24 L. J. Boucher, C. G. Coe, *Inorg. Chem.* **1975**, *14*, 1289.
25 S. R. Cooper, M. Calvin, *J. Am. Chem. Soc.* **1977**, *99*, 6623.
26 K. S. Hagen, W. H. Armstrong, H. Hope, *Inorg. Chem.* **1988**, *27*, 967.
27 K. J. Brewer, M. Calvin, R. S. Lumpkin, J. W. Otvos, L. O. Spreer, *Inorg. Chem.* **1989**, *28*, 4446.
28 H. J. Mok, J. A. Davis, S. Pal, S. K. Mandal, W. H. Armstrong, *Inorg. Chem. Acta* **1997**, *263*, 385.
29 H. Torayama, T. Nishide, H. Asada, M. Fujiwara, T. Matsushita, *Polyhedron* **1998**, *17*, 105.
30 B. C. Dave, R. S. Czernuscewicz, *Inorg. Chem. Acta* **1994**, *227*, 33.
31 J. M. North, R. M. Achey, N. S. Dalal, *Phys. Rev. B* **2002**, *66*, 174437.
32 J. M. North, L. J. van de Burgt, N. S. Dalal, *Solid State Commun.* **2002**, *123*, 75.
33 A. Cua, J. S. Vrettos, J. C. de Paula, G. W. Brudvig, D. F. Bocian, *J. Biol. Inorg. Chem.* **2003**, *8*, 439.
34 J. E. McGrady, R. Stranger, *J. Am. Chem. Soc.* **1997**, *119*, 8512.
35 T. Soda, Y. Kitagawa, T. Onishi, Y. Takano, Y. Shigeta, H. Nagao, Y. Yoshioka, K. Yamaguchi, *Chem. Phys. Lett.* **2000**, *319*, 223.
36 C. D. Delfs, R. Stranger, *Inorg. Chem.* **2001**, *40*, 3061.
37 G. Alluón, E. Ruiz, S. Alvarez, *Chem. Eur. J.* **2002**, *8*, 2508.
38 V. Barone, A. Bencini, D. Gatteschi, F. Totti, *Chem. Eur. J.* **2002**, *8*, 5019.
39 C. D. Delfs, R. Stranger, *Inorg. Chem.* **2003**, *42*, 2495.
40 S. Petrie, S. Mukhopadhyay, W. H. Armstrong, R. Stranger, *Phys. Chem. Chem. Phys.* **2004**, *6*, 4871.
41 S. Petrie, R. Stranger, *Inorg. Chem.* **2004**, *43*, 5237.
42 S. Sinnecker, F. Neese, L. Noodleman, W. Lubitz, *J. Am. Chem. Soc.* **2004**, *126*, 2613.
43 M. Lundberg, M. R. A. Blomberg, P. E. M. Siegbahn, *J. Phys. Chem. B* **2004**, *43*, 264.
44 M. Lundberg, P. E. M. Siegbahn, *J. Phys. Chem. B* **2005**, *109*, 10513.
45 P. E. M. Siegbahn, R. H. Crabtree, *J. Am. Chem. Soc.* **1999**, *121*, 117.
46 P. E. M. Siegbahn, M. R. A. Blomberg, *Annu. Rev. Phys. Chem.* **1999**, *50*, 221.
47 M. Lundberg, P. E. M. Siegbahn, *Phys. Chem. Chem. Phys.* **2004**, *6*, 4772.
48 M. J. Frisch, G. W. Trucks, H. B. Schlegel, G. E. Scuseria, M. A. Robb, J. R. Cheeseman, J. A. Montgomery, Jr., T. Vreven, K. N. Kudin, J. C. Burant, J. M. Millam, S. S. Iyengar, J. Tomasi, V. Barone, B. Mennucci, M. Cossi, G. Scalmani, N. Rega, G. A. Petersson, H. Nakatsuji, M. Hada, M. Ehara, K. Toyota, R. Fukuda, J. Hasegawa, M. Ishida, T. Nakajima, Y. Honda, O. Kitao, H. Nakai, M. Klene, X. Li, J. E. Knox, H. P. Hratchian, J. B. Cross, C. Adamo, J. Jaramillo, R. Gomperts, R. E. Stratmann, O. Yazyev, A. J. Austin, R. Cammi, C. Pomelli, J. W. Ochterski, P. Y. Ayala, K. Morokuma, G. A. Voth, P. Salvador, J. J. Dannenberg, V. G. Zakrzewski, S. Dapprich, A. D. Daniels, M. C. Strain, O. Farkas, D. K. Malick, A. D. Rabuck, K. Raghavachari, J. B. Foresman, J. V. Ortiz, Q. Cui, A. G. Baboul, S. Clifford, J. Cioslowski, B. B. Stefanov, G. Liu, A. Liashenko, P. Piskorz, I. Komaromi, R. L. Martin, D. J. Fox, T. Keith, M. A. Al-Laham, C. Y. Peng, A. Nanayakkara, M. Challacombe, P. M. W. Gill, B. Johnson, W. Chen, M. W. Wong, C. Gonzalez, J. A. Pople, *Gaussian 03, Revision C.02*, Gaussian, Inc., Wallingford CT, **2004**.
49 *Jaguar 5.5*, Schrödinger, L.L.C., Portland, OR, **1991–2003**.
50 A. D. Becke, *J. Chem. Phys.* **1993**, *98*, 5648.
51 J. P. Perdew, J. A. Chevary, S. H. Vosko, K. A. Jackson, M. R. Pederson, D. J. Singh, C. Fiolhais, *Phys. Rev. B* **1992**, *46*, 6671.
52 J. P. Perdew, K. Burke, Y. Wang, *Phys. Rev. B* **1996**, *54*, 16533.
53 P. J. Hay, W. R. Wadt, *J. Chem. Phys.* **1985**, *82*, 299.
54 T. Shimanouchi, *Computer Program of Normal Coordinate Treatement of Polyatomic Molecules*, The University of Tokyo, Tokyo, **1968**.
55 H. Yoshida, M. Tasumi, *J. Chem. Phys.* **1988**, *89*, 2803.
56 H. Visser, C. E. Dubé, W. H. Armstrong, K. Sauer, V. K. Yachandra, *J. Am. Chem. Soc.* **2002**, *124*, 11008.
57 J. E. Sheats, R. S. Czernuszewicz, G. C. Dismukes, A. L. Rheingold, V. Petrouleas, J. Stubbe, W. H. Armstrong, R. H. Beer, S. J. Lippard, *J. Am. Chem. Soc.* **1987**, *109*, 1435.